OPUS-HSO

Repositorium der Hochschule Offenburg
https://opus.hs-offenburg.de

Additively Manufactured Calibration Target for Intensity-Based LiDAR Calibration in Industrial Robotics

Thomas Wendt, Sinan Emre Süme, Andi Schnebel, Stefan Rupitsch

Zitiervorschlag im APA Stil:

Wendt, T., Süme, S. E., Schnebel, A., & Rupitsch, S. (2026). Additively Manufactured Calibration Target for Intensity-Based LiDAR Calibration in Industrial Robotics. *Tagungsband : 23. ITG/GMA-Fachtagung Sensoren und Messsysteme 2026*, 372–376. https://doi.org/10.5162/sensoren2026/M1-3.4

Abstract

Accurate extrinsic calibration of robot-mounted LiDAR sensors requires the extraction of unambiguous geometric features from the sensor data. Intensity-based corner detection is an established strategy, but it relies on a calibration target that provides a stable, high-contrast reflectivity pattern in the near-infrared spectrum. Conventional targets based on printed or painted checkerboards are subject to surface degradation and are restricted to planar geometries. The presented contribution proposes a calibration target fabricated by multi-material additive manufacturing, combining Reflect-O-Lay (a retroreflective PLA composite) and Fiberlogy PA□□+CF□□ (a carbon-fibre-reinforced polyamide) to produce a five by five checkerboard with intrinsic near-infrared reflectivity contrast at 940 nanometres. Due to the contrast embedded in the material composition, the target is inherently robust against abrasion, moisture, and ultraviolet exposure, and the additive manufacturing route permits arbitrary geometric modifications without tooling cost. Corner detection accuracy is evaluated experimentally on a RoboSense E□R solid-state LiDAR sensor mounted on a KUKA LBR iisy 11 R□□□□ manipulator. Across ten robot configurations, the detected inner corner positions agree with the nominal grid geometry to a Procrustes RMSE of 7.6 millimetres with a systematic spacing bias below half a percent, consistent with the ranging precision of the sensor. A comparison against reference targets reported in the literature places the proposed AM target in the same accuracy regime as established solutions while offering superior material stability and design flexibility.

Nutzungsbedingungen

Dieses Dokument wird unter diesen Bedinungen zur Verfügung gestellt:
Urheberrechtlich geschützt
Für weitere Informationen siehe:
https://rightsstatements.org/page/InC/1.0/

Kontakt

Hochschule Offenburg | Bibliothek
Badstraße 24
77652 Offenburg
Telefon: (0781) 205-240
E-Mail: bibliothek@hs-offenburg.de
www.hs-offenburg.de/bibliothek

10.5162/sensoren2026/M1-3.4

Additively Manufactured Calibration Target for Intensity-Based LiDAR Calibration in Industrial Robotics

Thomas M. Wendt[1], *Sinan Süme*[1], *Andi Schnebel*[1], *Stefan J. Rupitsch*[2]
[1] Offenburg University of Applied Sciences, Badstr. 24, 77656 Offenburg, Germany
[2] Laboratory for Electrical Instrumentation and Embedded Systems, Department of Microsystems Engineering, University of Freiburg, Georges-Köhler-Allee 106, 79110 Freiburg, Germany
sinan.sueme@hs-offenburg.de

Summary: Accurate extrinsic calibration of robot-mounted LiDAR sensors requires the extraction of unambiguous geometric features from the sensor data. Intensity-based corner detection is an established strategy, but it relies on a calibration target that provides a stable, high-contrast reflectivity pattern in the near-infrared spectrum. Conventional targets based on printed or painted checkerboards are subject to surface degradation and are restricted to planar geometries. The presented contribution proposes a calibration target fabricated by multi-material additive manufacturing, combining Reflect-O-Lay (a retroreflective PLA composite) and Fiberlogy PA12+CF15 (a carbon-fibre-reinforced polyamide) to produce a five by five checkerboard with intrinsic near-infrared reflectivity contrast at 940 nanometres. Due to the contrast embedded in the material composition, the target is inherently robust against abrasion, moisture, and ultraviolet exposure, and the additive manufacturing route permits arbitrary geometric modifications without tooling cost. Corner detection accuracy is evaluated experimentally on a RoboSense E1R solid-state LiDAR sensor mounted on a KUKA LBR iisy 11 R1300 manipulator. Across ten robot configurations, the detected inner corner positions agree with the nominal grid geometry to a Procrustes RMSE of 7.6 millimetres with a systematic spacing bias below half a percent, consistent with the ranging precision of the sensor. A comparison against reference targets reported in the literature places the proposed AM target in the same accuracy regime as established solutions while offering superior material stability and design flexibility.

Keywords: LiDAR calibration, additive manufacturing, multi-material FDM, intensity-based feature extraction, industrial robotics

Introduction

Three-dimensional LiDAR sensors are increasingly employed in robotic manufacturing cells for illumination-independent spatial perception tasks such as quality inspection, bin picking, and dimensional verification. Integrating such sensors into a robotic system requires that the sensor coordinate frame be precisely related to the robot kinematic chain, a problem known as *eye-in-hand extrinsic calibration*. The unknown flange-to-sensor transformation $\mathbf{X} \in SE(3)$ satisfies the classical hand-eye equation $\mathbf{AX} = \mathbf{XB}$, first established by Tsai and Lenz [1] and Shiu and Ahmad [2].

Target-based calibration methods commonly extract features by fitting the checkerboard as a dominant plane in the point cloud and deriving bounding edges as pose constraints [3, 4]. Such geometric approaches are fundamentally limited by the discrete angular sampling of the LiDAR beam pattern, which introduces quantization errors at target boundaries [5]. Intensity-based corner detection overcomes this limitation by exploiting the per-point reflectivity contrast between adjacent target regions [6, 7, 8], but presupposes a target with stable, high-contrast reflectivity in the operating wavelength of the sensor. Conventional painted or printed checkerboards rely on surface coatings whose optical properties are known to degrade under abrasion, humidity, and UV exposure [9], and alternative target geometries such as 3D towered checkerboards [10] or boards with circular cut-outs [11] require custom machining and remain restricted to a fixed geometry.

The present work proposes a multi-material AM calibration target in which the reflectivity contrast is intrinsic to the material composition. The contributions are:

- A multi-material AM target combining Reflect-O-Lay and PA12+CF15 that provides long-term reflectivity stability and geometric design freedom beyond the planar paradigm
- The characterization of the near-infrared reflectivity contrast at $940\,\mathrm{nm}$ obtained through the material combination
- An experimental evaluation of the corner detection accuracy achievable with this target on a solid-state LiDAR sensor, including a comparison against reference targets reported in the literature

Additively Manufactured Calibration Target

Material Selection

The target exploits the opposing near-infrared reflectivity of two commercially available FDM filaments at the RoboSense E1R operating wavelength of $\lambda = 940\,\mathrm{nm}$.

High-reflectivity constituent—Reflect-O-Lay (Lay Filaments, Germany) [12] is a semi-flexible PLA-based composite loaded

with retroreflective microsphere pigments. The retroreflective mechanism returns incident laser radiation towards its source with minimal angular deviation, independent of the angle of incidence, ensuring consistent high-intensity LiDAR returns across the full $\pm 40°$ tilt range. Processing parameters: extrusion temperature $210\,°$C, nozzle diameter ≥ 0.4 mm.

Low-reflectivity constituent—Fiberlogy PA12+CF15 (Fiberlab S.A., Poland) [13] is a polyamide-12 matrix reinforced with $15\,\%$ short carbon fibres. Carbon-fibre-filled polymers are established near-infrared absorbers at 940 nm [14], yielding consistently low LiDAR return intensities. The material additionally provides high dimensional stability and thermal resistance up to $160\,°$C. Processing parameters: extrusion temperature 255–$270\,°$C, heated bed 90–$110\,°$C, hardened-steel nozzle.

The reflectivity contrast ΔR is thereby embedded within the material composition, eliminating degradation mechanisms associated with abrasion, moisture absorption, and UV exposure that affect surface coatings.

Target Geometry

The target comprises a 5×5 checkerboard pattern with a field size of 45 mm $\times$ 45 mm, yielding $4 \times 4 = 16$ inner corner points as calibration landmarks. Including the surrounding border (4.5 mm width), the total plate dimensions are 234 mm $\times$ 234 mm, as displayed in Fig. 1.

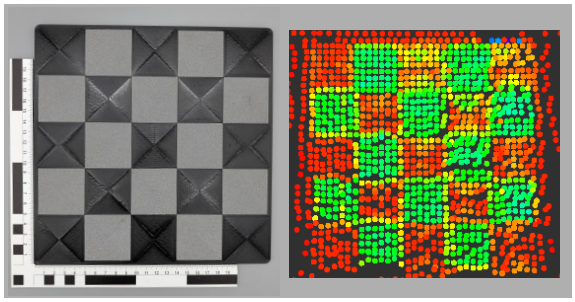

Fig. 1: AM multi-material calibration target. Light fields: Reflect-O-Lay. Dark fields: PA12+CF15 (left). E1R intensity image showing the reflectivity contrast ΔR at 940 nm (right).

At the design working distance of 0.4–1.2 m, the E1R angular resolution of $0.625°$ yields approximately 4–6 beam footprints per field boundary, sufficient for stable intensity-gradient computation across each material interface. The AM fabrication approach allows field size, board dimensions, and aspect ratio to be adapted to any sensor–distance combination by modifying the CAD model, without incurring tooling cost. Non-planar surface elements or mounting features may be incorporated within the same print job.

Calibration Framework

System Configuration and Kinematic Model

The experimental platform consists of a KUKA LBR iisy 11 R1300 six-axis collaborative manipulator with a RoboSense E1R solid-state LiDAR sensor attached to the flange.

Four coordinate frames are involved (Fig. 2):

- Robot base frame $\{B\}$
- Flange frame $\{F\}$ with pose $\mathbf{T}_{F,i} \in SE(3)$ from the KUKA controller
- Sensor frame $\{S\}$ related to $\{F\}$ by the unknown offset $\mathbf{X} \in SE(3)$
- Stationary target frame $\{P\}$.

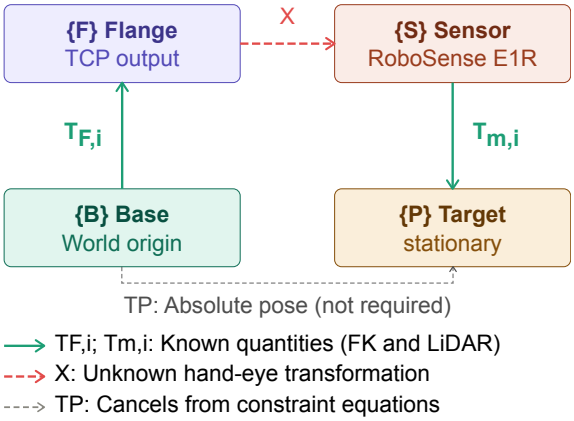

Fig. 2: Coordinate frames. Known: flange pose $\mathbf{T}_{F,i}$ (green). Unknown: hand-eye offset $\mathbf{X}$ (red). The absolute target pose $\mathbf{T}_P$ cancels from the estimation problem.

Since the target is stationary, the kinematic chain $\mathbf{T}_{F,i} \cdot \mathbf{X} \cdot \mathbf{T}_{m,i} = \mathbf{T}_P = \text{const}$ holds for all configurations i. Equating two configurations i, j and eliminating $\mathbf{T}_P$ yields the classical hand-eye equation:

$$\underbrace{\mathbf{T}_{F,j}^{-1}\mathbf{T}_{F,i}}_{\mathbf{A}_{ij}} \cdot \mathbf{X} \;=\; \mathbf{X} \cdot \underbrace{\mathbf{T}_{m,j}\,\mathbf{T}_{m,i}^{-1}}_{\mathbf{B}_{ij}}, \tag{1}$$

where $\mathbf{A}_{ij}$ is the relative flange motion from forward kinematics and $\mathbf{B}_{ij}$ the relative target displacement observed by the sensor. The absolute target pose cancels out and is neither measured nor required.

Intensity-Based Corner Detection

At each configuration, the E1R acquires a point cloud of the target. Each point carries a range value (resolution 5 mm) and an 8-bit intensity value (0–255), where Reflect-O-Lay fields produce high and PA12+CF15 fields produce low return intensities. The processing pipeline operates as follows:

1. **Intensity image formation.** Per-point intensity values are projected onto a regular angular grid ($0.625°$ spacing) using the known sensor beam geometry, yielding a 197×143 pixel intensity image.
2. **Region-of-interest extraction.** The target region is segmented by intensity thresholding (fraction 0.30 of the image maximum) followed by morphological filtering.
3. **Corner detection.** The intensity image is upscaled by a factor of 8 (bicubic interpolation), binarised (Otsu thresholding), and processed with `findChessboardCornersSB` [15] with subpixel refinement. Multiple preprocessing variants (Gaussian blur kernels, polarity inversion) are attempted.
4. **3D back-projection.** Each detected 2D corner is mapped back to 3D by intensity-weighted averaging of the neighbouring point cloud returns within a $\pm 1.2°$ angular window.

The result is a set of 16 corner positions $\mathbf{c}_k^{(i)} \in \mathbb{R}^3$ ($k = 1, \ldots, 16$) per detected pose, expressed in the sensor coordinate frame.

Parameter Estimation

Rather than constructing intermediate target-pose matrices $\mathbf{T}_{m,i}$ from the detected corners, a direct scatter minimisation approach is employed. For a candidate $\mathbf{X} \in SE(3)$, each corner is projected to the base frame:

$$\mathbf{p}_k^{(i)} = \mathbf{T}_{F,i} \cdot \mathbf{X} \cdot \mathbf{c}_k^{(i)}. \tag{2}$$

Since the target is stationary, $\mathbf{p}_k^{(i)}$ should be identical across all poses i for each corner k. The optimal $\hat{\mathbf{X}}$ is obtained by minimizing total scatter:

$$\hat{\mathbf{X}} = \arg\min_{\mathbf{X} \in SE(3)} \sum_{k=1}^{16} \sum_{i=1}^{N_{\text{eval}}} \left\| \mathbf{p}_k^{(i)} - \bar{\mathbf{p}}_k \right\|^2, \tag{3}$$

where $\bar{\mathbf{p}}_k = \frac{1}{N_{\text{eval}}} \sum_i \mathbf{p}_k^{(i)}$ is the mean position of corner k across all N_{eval} evaluated poses. This formulation uses all $16 \times N_{\text{eval}}$ corner observations equally and avoids the error-prone construction of 6-DoF target-pose matrices from subsets of corners. The optimisation is solved by Levenberg–Marquardt initialised from the identity.

Experimental Results

A total of $N_{\text{total}} = 20$ robot configurations are collected, distributed to ensure variation in all six degrees of freedom with translational offsets of $0.4\,\text{m} - 1.0\,\text{m}$ and angular tilts up to $\pm 40°$ about the target normal. For each configuration, a static point cloud is acquired. After applying the processing pipeline, $N_{\text{eval}} = 10$ poses covering the full intended working envelope (sensor-to-target distance $0.46\,\text{m} - 1.01\,\text{m}$) are retained for the accuracy analysis. The remaining configurations include cases at extreme viewing angles or low point density and are excluded from the quantitative evaluation; extending the approach to such limiting conditions is discussed in the Conclusions.

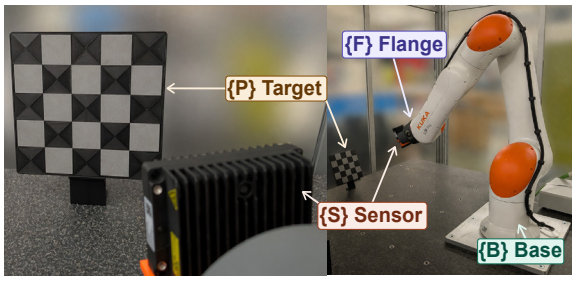

Fig. 3: Experimental setup. KUKA LBR iisy 11 R1300 with RoboSense E1R on the flange and AM target at a fixed position.

Corner Detection Accuracy

The primary metric is the Procrustes fit: for each detected pose, the 16 corner positions in sensor coordinates are rigidly aligned (rotation and translation, no scaling) to the nominal 4×4 grid ($45\,\text{mm}$ spacing). Tab. 1 reports the per-pose residuals.

Tab. 1: Corner detection accuracy per pose. Procrustes RMSE and maximum per-corner error (rigid alignment to nominal 4×4 grid with 45 mm spacing, no scaling).

Pose	d (m)	RMSE (mm)	Max. (mm)
1	0.73	6.3	11.4
2	1.01	8.6	13.5
3	0.83	7.3	13.6
4	0.64	9.4	15.7
5	0.49	8.1	14.8
6	0.66	8.1	14.8
7	0.52	8.2	13.8
8	0.82	6.6	12.9
9	0.46	6.1	12.4
10	0.61	7.1	16.2
Mean	**0.68**	**7.6**	**13.9**
Std.	**0.18**	**1.0**	**1.4**

Across all ten evaluated poses (sensor-to-target distance $0.46\,\text{m} - 1.01\,\text{m}$), the Procrustes RMSE is $7.6 \pm 1.0\,\text{mm}$ with a maximum per-corner error of $13.9 \pm 1.4\,\text{mm}$.

Grid Geometry Consistency

As a complementary metric independent of rigid-body fitting, the inter-corner spacings are compared directly to the nominal value. Across all 240 adjacent-corner distances (horizontal and vertical) from the ten evaluated poses, the measured mean spacing is $45.18\,\text{mm}$ (nominal:

Tab. 2: Comparison of reference calibration targets for LiDAR. Reported accuracy values refer to corner- or feature-localization RMSE on the target surface; values are approximated from the cited references and depend on sensor and distance.

Reference	Fabrication	Contrast source	Accuracy (mm)
Pandey et al. [3]	Printed paper on board	Ink reflectance	∼10–20
Zhou et al. [4]	Printed checkerboard	Ink reflectance	∼10–15
Beltrán et al. [11]	Milled planar board with cut-outs	Geometric (depth edges)	∼15
Ren et al. [10]	Stacked planar boards (3D tower)	Printed pattern	∼8–12
Kaasalainen et al. [9]	Natural reference samples	Material reflectance	n/a (intensity ref.)
This work	**Multi-material AM checkerboard**	**Material reflectance**	**7.6 ± 1.0**

45.0 mm), corresponding to a systematic bias of $+0.18$ mm ($+0.4\,\%$) with a standard deviation of 5.8 mm. The planarity of the detected grid (distance of each corner from the best-fit plane through the 16 points) yields an RMSE of 5.2 ± 1.1 mm. Both the spacing deviation and the out-of-plane scatter are consistent with the specified ranging precision of the E1R sensor (± 50 mm at 1σ), confirming that the observed corner position errors are dominated by sensor noise rather than systematic target artefacts.

Multi-Pose Consistency

In order to assess the repeatability of the cross-pose corner extraction, the detected corners from all ten evaluated poses are transformed into a common reference frame using the measured flange pose and the estimated flange-to-sensor offset $\hat{\mathbf{X}}$ from Eq. (3). For each of the 16 corners, the scatter of the ten observations around their mean position is evaluated. The resulting overall RMSE is 10.9 mm across all $16 \times 10 = 160$ projected corner positions, which is consistent with the single-pose Procrustes RMSE combined with the specified ranging precision of the E1R sensor and confirms that corner extraction is reproducible across the workspace.

Comparison with Target References

Tab. 2 compares the proposed AM target against a representative selection of calibration targets reported in the recent literature [3, 4, 11, 10, 9]. The comparison considers the target fabrication route, the source of the reflectivity contrast, and the reported corner or feature localization accuracy. The comparison is intended to situate the proposed target within the established accuracy regime rather than to identify a single best performer, since absolute accuracy figures are influenced by the LiDAR angular resolution and working distance.

The proposed AM target achieves corner localization within the accuracy range reported for established printed or machined targets [3, 4, 11, 10], while offering two distinctive features. First, the reflectivity contrast originates from the bulk material rather than from a surface coating, following the rationale of material-based radiometric reference targets [9] and thereby avoiding the coating-degradation mechanisms identified as a limitation of printed checkerboards. Second, the AM fabrication route allows the target geometry , field size, aspect ratio, or out-of-plane features to be reconfigured through the CAD model without any tooling-related cost, a flexibility that machined planar boards [11] or stacked 3D targets [10] cannot provide.

Conclusions

A multi-material additively manufactured calibration target has been proposed and experimentally evaluated for intensity-based LiDAR corner detection in an eye-in-hand robotic configuration. Through the combination of Reflect-O-Lay and PA12+CF15 as retroreflective and absorptive constituents, a stable near-infrared intensity contrast is embedded within the material composition, eliminating reliance on surface coatings and the associated degradation mechanisms. The 5×5 checkerboard with 45 mm field size provides 16 inner calibration corners that are automatically detectable by standard algorithms applied to the LiDAR intensity channel.

Experimental evaluation on a RoboSense E1R sensor ($\lambda = 940$ nm, angular resolution $0.625°$) mounted on a KUKA LBR iisy 11 R1300 yields a corner detection accuracy of 7.6 ± 1.0 mm (Procrustes RMSE) with a spacing bias below $0.5\,\%$ and a multi-pose repeatability of 10.9 mm RMSE. The observed accuracy is consistent with the specified ranging precision of the sensor and places the proposed AM target within the accuracy range reported for established printed, milled, and stacked calibration targets, while offering superior material stability and geometric design freedom.

Future work will exploit the design freedom of additive manufacturing to produce non-planar target geometries, including tilted, stepped, or multi-facet arrangements, that are expected to improve feature observability at extreme viewing angles and reduce the number of required robot configurations. Higher-resolution LiDAR sensors are also expected to lower the corner localization error below the current sensor-noise-limited regime.

References

[1] R. Y. Tsai and R. K. Lenz, A new technique for fully autonomous and efficient 3D robotics hand/eye calibration, *IEEE Trans. Robot. Autom.* 5, 345–358 (1989); doi: 10.1109/70.34770

[2] Y. C. Shiu and S. Ahmad, Calibration of wrist-mounted robotic sensors by solving homogeneous transform equations of the form AX=XB, *IEEE Trans. Robot. Autom.* 5, 16–29 (1989); doi: 10.1109/70.88014

[3] G. Pandey, J. R. McBride, S. Savarese, and R. M. Eustice, Extrinsic calibration of a 3D laser scanner and an omnidirectional camera, *IFAC Proc. Vol.* 43, 336–341 (2010); doi: 10.3182/20100906-3-IT-2019.00059

[4] L. Zhou, Z. Li, and M. Kaess, Automatic extrinsic calibration of a camera and a 3D LiDAR using line and plane correspondences, *Proc. IEEE/RSJ Int. Conf. Intell. Robots Syst. (IROS)*, 5562–5569 (2018); doi: 10.1109/IROS.2018.8593660

[5] Q. Zhang and R. Pless, Extrinsic calibration of a camera and laser range finder (improves camera calibration), *Proc. IEEE/RSJ Int. Conf. Intell. Robots Syst. (IROS)*, 2301–2306 (2004); doi: 10.1109/IROS.2004.1389752

[6] J. Levinson and S. Thrun, Automatic online calibration of cameras and lasers, *Robotics: Science and Systems IX* (2013); doi: 10.15607/RSS.2013.IX.029

[7] M. Mattamala, J. Frey, P. Libera, N. Chebrolu, G. Martius, C. Cadena, M. Hutter, and M. Fallon, Extrinsic calibration of camera to LiDAR using a differentiable checkerboard model, *Proc. IEEE/RSJ Int. Conf. Intell. Robots Syst. (IROS)*, 10404–10411 (2023); doi: 10.1109/IROS55552.2023.10341383

[8] W. Wang, K. Sakurada, and N. Kawaguchi, Reflectance intensity assisted automatic and accurate extrinsic calibration of 3D LiDAR and panoramic camera using a printed chessboard, *Remote Sensing* 9, 851 (2017); doi: 10.3390/rs9080851

[9] S. Kaasalainen et al., Radiometric calibration of LIDAR intensity with commercially available reference targets, *IEEE Trans. Geosci. Remote Sens.* 47, 588–598 (2009); doi: 10.1109/TGRS.2008.2003351

[10] F. Ren et al., Extrinsic calibration of camera and LiDAR systems with three-dimensional towered checkerboards, *Int. J. Intell. Syst.* 2024, 2478715 (2024); doi: 10.1155/2024/2478715

[11] J. Beltrán, C. Guindel, A. de la Escalera, and F. García, Automatic extrinsic calibration method for LiDAR and camera sensor setups, *IEEE Trans. Intell. Transp. Syst.* 23, 17677–17689 (2022); doi: 10.1109/TITS.2022.3155228

[12] K. Parthy, Reflect-O-Lay: Retroreflective FDM filament—product description and print parameters, Lay Filaments, Germany (2015). Available: `https://filament2print.com/en/pla/690-reflect-o-lay.html`

[13] Fiberlab S.A., Fiberlogy Nylon PA12+CF15: Technical datasheet, Pruszków, Poland (2023). Available: `https://fiberlogy.com/en/Nylon-PA12CF15-Filament`

[14] C. Amendola et al., Optical characterization of 3D-printed PLA and ABS filaments for diffuse optics applications, *PLOS ONE* 16, e0253181 (2021); doi: 10.1371/journal.pone.0253181

[15] G. Bradski, The OpenCV Library, *Dr. Dobb's Journal of Software Tools* (2000). Available: `https://opencv.org`